Tidal deformability of an anisotropic compact star: Implications of GW170817

Bhaskar Biswas[1,*] and Sukanta Bose[1,2]

[1]*Inter-University Centre for Astronomy and Astrophysics, Post Bag 4, Ganeshkhind, Pune 411 007, India*
[2]*Department of Physics & Astronomy, Washington State University, 1245 Webster, Pullman, Washington 99164-2814, USA*

We use gravitational wave (GW) and electromagnetic (EM) observations of GW170817 to constrain the extent of pressure anisotropy in it. While it is quite likely that the pressure inside a neutron star is mostly isotropic, certain physical processes or characteristics, such as phase transitions in nuclear matter or the presence of strong magnetic fields, can introduce pressure anisotropy. In this work, we show that anisotropic pressure in neutron stars can reduce their tidal deformability substantially. For the anisotropy-pressure model of Bowers and Liang and a couple of relativistic EOSs—DDHδ and GM1—we demonstrate that this reduction in spherical neutron stars with masses in the range of 1 to 2 $M_\odot$ can be 23% to 46%. This suggests that certain EOSs that are ruled out by GW170817 observations, under assumptions of pressure isotropy, can become viable if the stars had a significant enough anisotropic pressure component, but do not violate causality. We also show how the inference of the star radius can be used to rule out certain EOSs (such as GM1), even for high anisotropic pressure, because their radii are larger than what the observations find.

I. INTRODUCTION

The recent detection of gravitational waves (GWs) from the binary neutron star (BNS) merger event GW170817 [1] has initiated a new way to probe and constrain the equation of state of compact stars [2,4]. In the inspiral stage of the binary coalescence the tidal deformation of the orbiting stars leaves an imprint on the emitted GW signal [5–8]. This imprint carries information about the composition of the star. Unfortunately, properties of neutron star matter at very high density are not fully understood. Therefore, modeling the star requires one to make certain assumptions about its interior.

One of the most common assumptions made in studies of the equilibrium structure of a neutron star is that its pressure is isotropic. Specifically, in a spherically symmetric neutron star, the radial pressure and the transverse pressure are taken to be equal. Interestingly, it has been argued in other studies that this equality may not always hold; in other words, the pressure in a neutron star can have an anisotropic component. In basic terms, pressure anisotropy can arise whenever the velocity distribution of particles in a fluid is anisotropic, which in turn can owe its origin to the presence of magnetic fields, turbulence, convection, etc., [9]. There are several studies (see, e.g., Refs. [10–12]) that suggest that at very high densities

relativistic interactions between nucleons can make the pressure anisotropic. In the density range of 0.2 fm^{-3} to 1 fm^{-3}, superdense nuclear matter makes a phase transition to almost equal numbers of protons, neutrons and π^- particles [13]. The π^- particles condense to a plane wave state of momentum that can be as large as $\approx$170 Mev/c. This condensation causes a drastic reduction in pressure, which softens the equation of state along the radial direction [14].

Another interesting scenario arises owing to strong magnetic fields that neutron stars are known to possess. Indeed, many neutron stars have magnetic fields with strength 10^{12}–10^{13} G; and there is evidence for the existence of supermagnetized neutron stars with magnetic fields as large as 10^{14}–10^{15} G [15,16]. Magnetic pressure associated with such strong magnetic fields can also induce pressure anisotropy.

Presence of P type superfluid or solid core can also introduce pressure anisotropy [10], where interactions among the P type superfluid nucleons produce the anisotropy. It has been shown by Herrera *et al.* [9] that use of the two-fluid model naturally predicts pressure anisotropy. An example of the two-fluid model is Superfluid Helium II, in the context of the Landau theory [17].

Finally, it is also known that in certain braneworld models of gravity, with an extra spatial dimension, the corrections induced in Einstein's equations on the

*bhaskarb@iucaa.in

four-dimensional brane can be modeled as a stress energy tensor with anisotropic pressure [18].

For the aforementioned reasons we explore here how gravitational wave observations of binary neutron stars and, in the process, measurements of their macroscopic parameters, such as their mass, radius and the tidal deformability parameter [5,6], can be used to test the presence or absence of pressure anisotropy in these stars. There exists a large body of work on equilibrium configuration and oscillations of anisotropic neutron stars [19–41]. These studies suggest that anisotropy in pressure, if present with a non-negligible magnitude, can have a significant effect on the mass-radius relationship and, therefore, the compactness of the star. That in turn leads one to enquire what effect, if any, anisotropy may have on the GWs emitted during a binary coalescence.

Yagi and Yunes [37] came close to addressing this matter when they compared the tidal deformability of slowly rotating neutron stars in the presence and absence of pressure anisotropy. Their work was mainly focused on how much the anisotropy affects the universal relation between moment of inertia, tidal Love number and quadrupole moment. In this present work we calculate the tidal deformability [6] of a static anisotropic compact star whose background is taken to be spherically symmetric. We also use a different EOS for pressure anisoptropy, namely, the one pioneered by Bowers and Liang [19]. We show that there are regions in that EOS parameter space that give rise to unphysical stellar configurations (owing to the existence of regions where causality would be violated). After discarding such configurations from further study, we calculate the change in the tidal deformability parameter of neutron stars for a few cases of anisotropic pressure EOS, in an otherwise standard relativistic equation of state (EOS). We find that the presence of pressure anisotropy generally reduces its tidal deformability, for a fixed stellar mass. We demonstrate how this property allows certain relativistic EOSs, for a range of pressure anisotropy magnitudes, to remain viable in light of GW170817. We also use that observation and universality relations between the tidal deformability parameter and stellar compactness, deduced here, to constrain the pressure anisotropy parameter. Finally, we explain how future observations of GWs from binary neutron stars can tighten this constrain further.

Throughout this paper, we set the gravitational constant G and the speed of light in vacuum c to unity, except when computing observational quantities, such as the second Love number or the tidal deformability parameter, for comparison with observations.

II. EQUILIBRIUM CONFIGURATIONS OF ANISOTROPIC COMPACT STARS

We consider a static, spherically symmetric fluid distribution with an anisotropic component. Its stress-energy tensor is given as:

$$T^\mu_\nu = \text{diag}(\rho, -p_r, -p_t, -p_t), \qquad (1)$$

where ρ is the density, and the transverse pressure p_t differs from the usual radial pressure p_r owing to anisotropy. In Schwarzschild coordinates the metric takes the form

$$ds^2 = g^{(0)}_{\alpha\beta} dx^\alpha dx^\beta = e^\nu dt^2 - e^\lambda dr^2 - r^2 d\theta^2 - r^2 \sin^2\theta d\varphi^2. \qquad (2)$$

Using this matter distribution and spacetime geometry in Einstein's equations gives one the following modified Tolman-Oppenheimer-Volkov (TOV) equations,

$$\frac{dp_r}{dr} = -\frac{(\rho + p_r)(m + 4\pi r^3 p_r)}{r(r - 2m)} + \frac{2}{r}(p_t - p_r), \qquad (3)$$

$$\frac{dm}{dr} = 4\pi r^2 \rho, \qquad (4)$$

where $m(r)$ is the mass enclosed within areal radius r.

To close this system of equations one considers two separate EOSs for p_r and p_t. We will assume barotropic EOS for radial pressure, $p_r = p_r(\rho)$. Specifically, we study stars with two different EOSs based on the relativistic mean field (RMF) parametrization, namely, DDHδ [42] and GM1 [43] in beta equilibrium. In both cases, for the crust an EOS by Douchin and Haensel [44] is added below a density of 10^{-3} fm^{-3}. For transverse pressure, we consider the functional form given by Bowers and Liang [19],

$$p_t = p + \frac{1}{3}\lambda_{BL} \frac{\rho + 3p}{1 - 2m/r}(\rho + p)r^2, \qquad (5)$$

where the constant λ_{BL} is a measure of anisotropy. Note that in Eq. (5), and hereafter, we use $p \equiv p_r$ to denote the radial pressure. For this particular choice of anisotropic EOS, the pressure anisotropy $(p_t - p)$ [which affects the second term on the right-hand side of Eq. (3)] must vanish quadratically with r at the center of the star in order to yield regular stellar solutions. This form of p_t was also motivated in Ref. [19] by the consideration that at least a part of the anisotropy is gravitationally induced, thereby, giving rise to its nonlinear dependence on p. The boundary condition $p(r = R) = 0$ determines the radius R of the star. For all physically acceptable solutions we must have $p, p_t \geq 0$ inside the star.

Following Silva et al. [36] we begin by examining solutions in the relatively narrow range $-2 \leq \lambda_{BL} \leq 2$ around isotropy, which is when $\lambda_{BL} = 0$. For DDHδ and GM1, we find that when the transverse pressure is higher than the radial pressure (i.e., $\lambda_{BL} > 0$) the star can support more mass against gravitational collapse compared to the opposite situation (i.e., $\lambda_{BL} < 0$). We also find that, for a fixed central density, compactness of the star increases
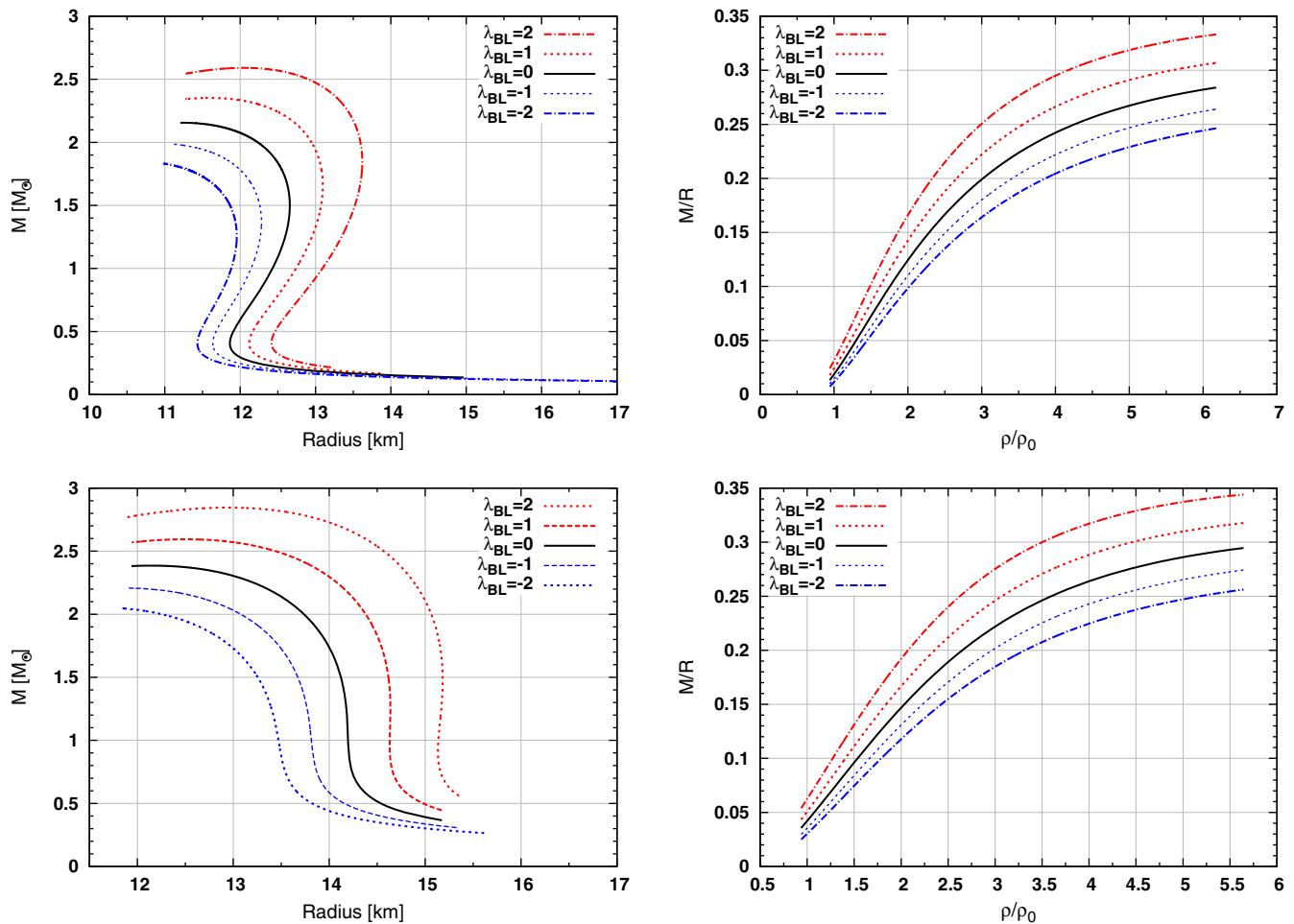
FIG. 1. The mass-radius relationship (left panel) and compactness of the neutron star as a function of normalized baryon density (right panel) for several values of the anisotropic parameter λ_{BL} using EOSs DDHδ (top panel) and GM1 (bottom panel).

(decreases) if the transverse pressure exceeds (falls below) radial pressure. These properties are depicted in Fig. 1. Is it possible to observationally constrain the degree of anisotropy in a neutron star? Below we present a way to do so with gravitational wave observations.

Focusing first on *negative* values of λ_{BL}, we find some evidence that the transverse pressure in such configurations may not always be positive. (See Fig. 2 for $\lambda_{BL} = -1, -2$.) Since these may correspond to unphysical solutions, we choose to study them in a separate work. However, for smaller negative values of λ_{BL}, the condition $p_t \geq 0$ can be respected everywhere in the star. Nevertheless, in those cases the anisotropic effects will be smaller; we do not study such cases here. Below we exclusively study the positive λ_{BL} solutions, with particular attention on how their tidal deformability may differ from the corresponding $\lambda_{BL} = 0$ solutions.

In Fig. 3 both radial pressure and transverse pressure are plotted as functions of r for the central baryon density $\rho = 5\rho_0$ (chosen arbitrarily) using DDHδ EOS for the positive values of $\lambda_{BL} = 1$ and 2. In both cases, we see

transverse pressure does not differ drastically from the radial pressure. Therefore, the amount of anisotropy that is allowed in this work is quite reasonable and also does not violate causality.

III. COMPUTATION OF TIDAL DEFORMABILITY

In the presence of an external tidal field ϵ_{ij} the equilibrium configuration of a neutron star gets tidally deformed. As a result the spherically symmetric star develops a quadrupole moment Q_{ij}. To linear order in ϵ_{ij}, this induced response of the body is described as

$$Q_{ij} = -\lambda \epsilon_{ij}, \tag{6}$$

where λ is tidal deformability of the neutron star and is related to the dimensionless second Love number k_2 as $\lambda = \frac{2}{3} k_2 R^5$. We also denote the mass of the star as M. To determine k_2, we study linear perturbation of the background metric following Thorne and Campolattaro [45]:
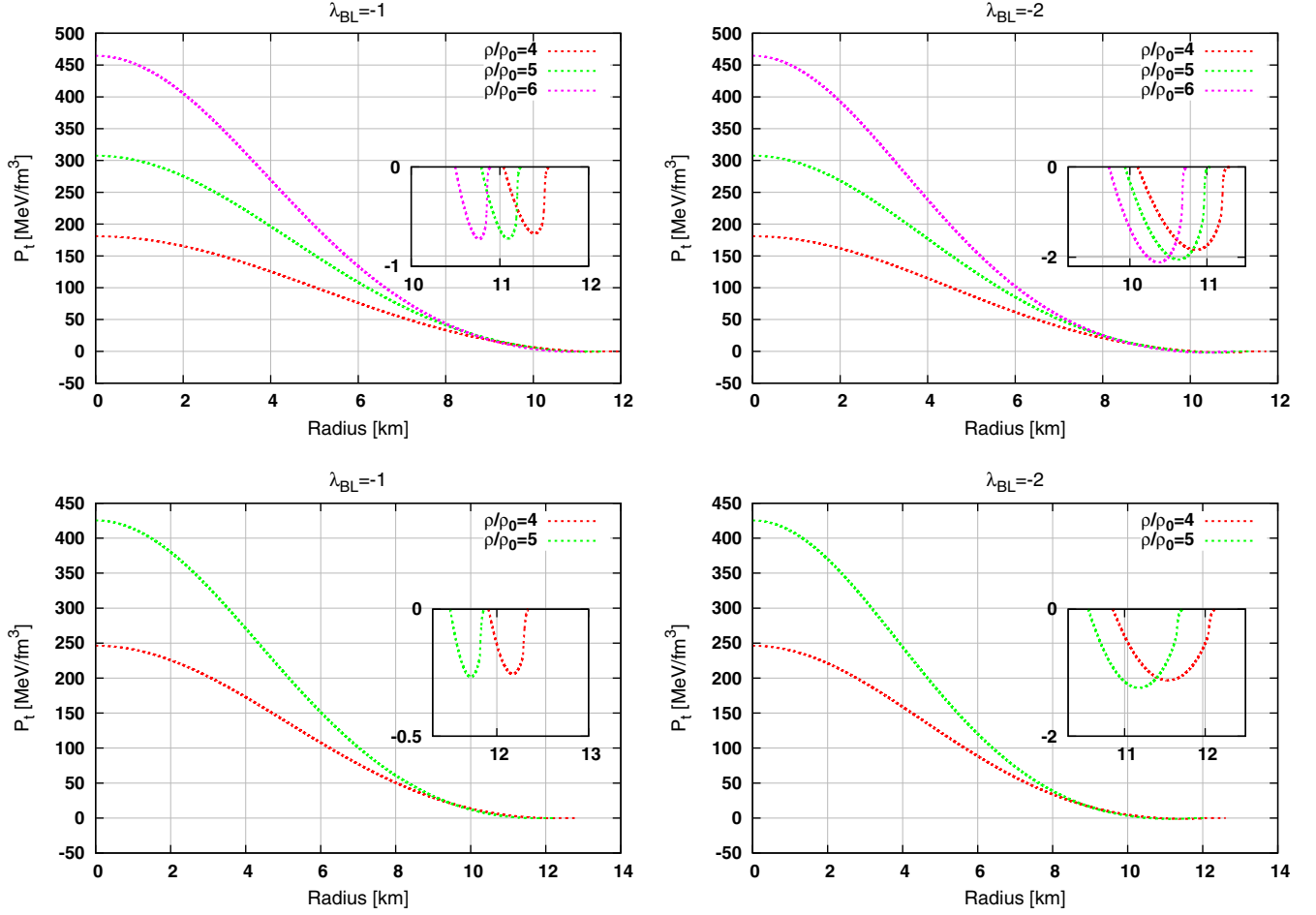
FIG. 2. Radial profile of transverse pressure for different values of central density using DDHδ (top panel) and GM1 (bottom panel) EOS: $\lambda_{BL} = -1$ (left panel) and $\lambda_{BL} = -2$ (right panel).
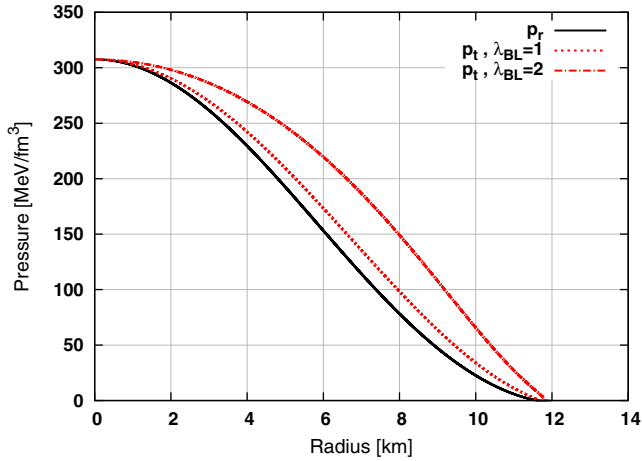

FIG. 3. Comparison of radial pressure and transverse pressure as functions of r for $\lambda_{BL} = 1$ and $\lambda_{BL} = 2$ using DDHδ EOS for the central density $\rho = 5\rho_0$. In both cases, the transverse pressure remains within a factor of a few of the radial pressure and does not violate causality. As we study later, even smaller values of the transverse pressure can have observational consequences.

$$g_{\alpha\beta} = g^{(0)}_{\alpha\beta} + h_{\alpha\beta}, \qquad (7)$$

where $h_{\alpha\beta}$ is the linearized perturbed metric. We expand components of metric and fluid perturbation variables in terms of spherical harmonics Y_{lm} [46]. We restrict ourselves to even parity perturbation for fixed values of l and m. Since we are interested only in quadrupolar deformation we set $l = 2$, and the result is independent of the choice of m [6]. With these restrictions the perturbed metric becomes

$$h_{\alpha\beta} = \mathrm{diag}[H_0(r)e^\nu, H_2(r)e^\lambda, r^2 K(r), r^2\sin^2\theta K(r)]$$
$$\times Y_{2m}(\theta, \varphi), \qquad (8)$$

where H_0, H_2, and K are all radial functions determined by the perturbed Einstein equations.

Expansion of the perturbed stress-energy tensor gives us the following relations: $\delta T^0_0 = \delta\rho = \frac{d\rho}{dp}\delta p$, $\delta T^r_r = -\delta p$ and $\delta T^\theta_\theta = \delta T^\varphi_\varphi = -\delta p_t = -\frac{dp_t}{dp}\delta p$. We insert these fluid and metric perturbations in linearized Einstein equations $\delta G^\beta_\alpha = 8\pi\delta T^\beta_\alpha$. From $\delta G^\theta_\theta - \delta G^\varphi_\varphi = 0$ and $\delta G^r_\theta = 0$ we get

$H_0 = H_2 \equiv H$ and $K' = H\nu' + H'$, respectively. By subtracting the equation $\delta G_\theta^\theta + \delta G_\varphi^\varphi = -16\pi \delta p_t$ from the tt-component of the perturbed Einstein equations we obtain the following differential equation for H:

$$H'' + H'\left[\frac{2}{r} + e^\lambda\left(\frac{2m(r)}{r^2} + 4\pi r(p-\rho)\right)\right]$$
$$+ H\left[4\pi e^\lambda\left(4\rho + 8p + \frac{\rho+p}{Ac_s^2}(1+c_s^2)\right) - \frac{6e^\lambda}{r^2} - \nu'^2\right]$$
$$= 0, \quad (9)$$

where $A \equiv \frac{dp_t}{dp}$, and $c_s^2 \equiv \frac{dp}{d\rho}$ is the speed of sound squared; moreover, the prime denotes derivative with respect to r. If we put $A = 1$ in Eq. (9) we recover the familiar master equation for the isotropic case [6].

Tidal Love number can be calculated by matching the internal solution with the external solution of the perturbed variable H at the surface of the star [6–8]. Then the value of tidal Love number can be found in terms of y and compactness parameter $C = \frac{M}{R}$:

$$k_2 = \frac{8}{5}(1-2C)^2 C^5 [2C(y-1)-y+2]\Big[2C(4(y+1)C^4$$
$$+ (6y-4)C^3 + (26-22y)C^2 + 3(5y-8)C - 3y+6)$$
$$- 3(1-2C)^2(2C(y-1)-y+2)\ln\left(\frac{1}{1-2C}\right)\Big]^{-1},$$
$$(10)$$

where y depends on the value of H and its derivative at the surface:

$$y = \frac{rH'}{H}\Big|_R.$$

In the left panel of Fig. 4, the tidal Love number k_2 is plotted as a function of mass for positive λ_{BL} using DDHδ (top panel) and GM1 (bottom panel). The isotropic case corresponds to $\lambda_{BL} = 0$. We observe that as λ_{BL} increases, the tidal Love number at a constant stellar mass decreases for both EOSs. In the right panel of Fig. 4 the dimensionless tidal deformability $\Lambda \equiv \lambda/M^5$ is plotted as a
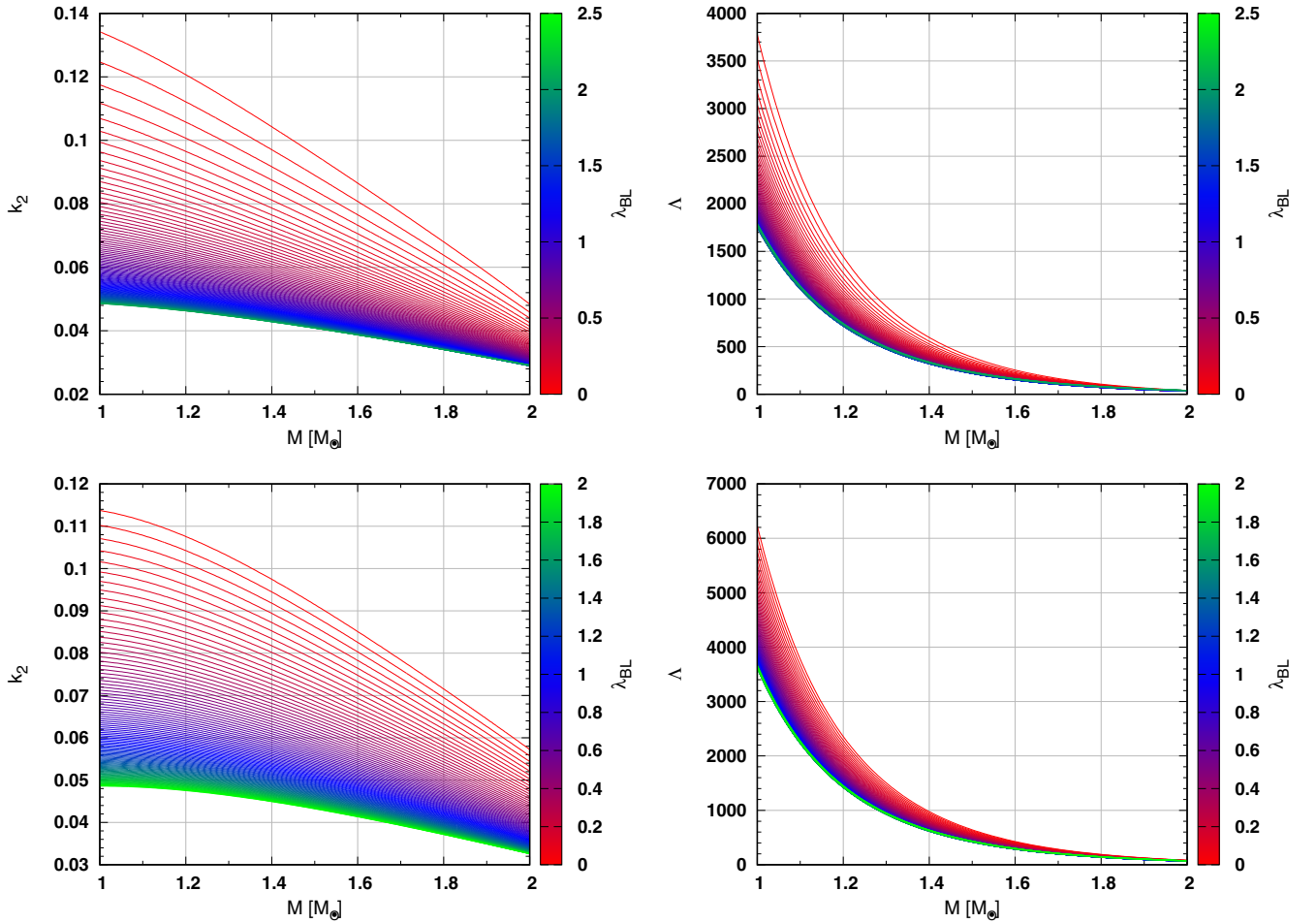

FIG. 4. Tidal Love number k_2 (left panel) and dimensionless tidal deformability Λ (right panel) are plotted as functions of mass using EOSs DDHδ (top panel) and GM1 (bottom panel) for positive values of λ_{BL}.

function of the star's mass between $1\,M_\odot$ to $2\,M_\odot$. We observe that positive anisotropy reduces the value of Λ, for a given mass.

IV. IMPLICATIONS OF GW170817 ON EOS WITH ANISOTROPIC PRESSURE

At leading order $\Lambda_{1,2}$ appear in the gravitational wave phase through the effective tidal deformability

$$\bar{\Lambda} = \frac{16}{13}\frac{(m_1 + 12m_2)m_1^4\Lambda_1 + (m_2 + 12m_1)m_2^4\Lambda_2}{(m_1 + m_2)^5}, \quad (11)$$

where Λ_1 and Λ_2 are the tidal deformabilities of the heavier and lighter stars, respectively. The recent detection of GWs from the binary neutron star merger event GW170817 has constrained $\bar{\Lambda}$ to be ≤ 720 [2,3] at 90% confidence level for low spin (dimensionless spin magnitude ≤ 0.05) prior. The corresponding chirp mass, $M_c = \frac{(m_1 m_2)^{3/5}}{(m_1 + m_2)^{1/5}}$, was measured to be $1.188^{+.004}_{-.002}\,M_\odot$ and

the mass ratio, $q = \frac{m_2}{m_1}$, was constrained between 0.7-1 for low spin prior. Also the EM counterpart of GW170817, named AT2017gfo, provides an additional constraint of $\bar{\Lambda} \geq 400$ [4]. Indeed, constraints from chiral effective field theory and perturbative quantum chromodynamics suggest for a lower bound on Λ that is as low as 120 for $1.4\,M_\odot$ [47]. As we show below, a lower value of $\Lambda_{1,2}$ and, therefore, $\bar{\Lambda}$, can allow for a larger range of λ_{BL} to be admissible by GW170817 observations. Here, we choose to be conservative and take $\bar{\Lambda} \geq 400$. Combining these GW and EM constraints gives the allowed range of $\bar{\Lambda}$ to be $400 \leq \bar{\Lambda} \leq 720$.

Many of the relativistic equations of state struggle to satisfy the upper bound, $\bar{\Lambda} \leq 720$ (see, e.g., Ref. [48]), assuming $\lambda_{BL} = 0$. That situation changes if anisotropy in pressure is present. In the left panel of Fig. 5, we have plotted $\bar{\Lambda}$ as a function of q for positive λ_{BL} using both DDHδ (upper panel) and GM1 (lower panel) EOSs. The allowed ranges of $\bar{\Lambda}$ are shaded in gray. Figure 5 shows
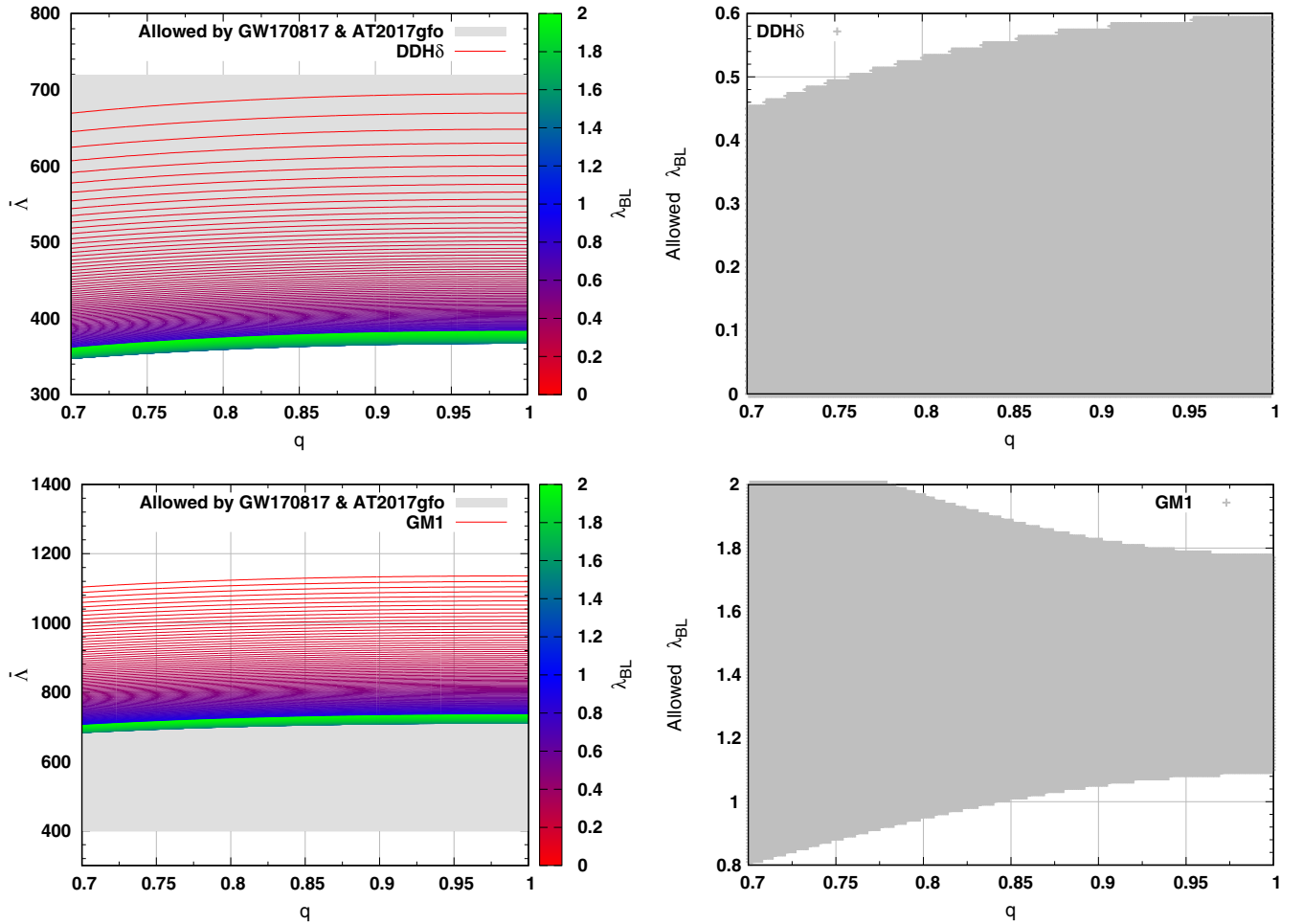

FIG. 5. $\bar{\Lambda}$ (left panel) and allowed values of λ_{BL} are plotted as functions of the mass ratio q for DDHδ (upper panel) and GM1 (lower panel) EOSs. The shaded regions in the left panel are allowed by GW-EM observations of GW170817 and AT2017gfo. In the right panel, the points cover the ranges of allowed λ_{BL} for various mass-ratio (q) values.

that between GM1 and DDHδ, only the latter satisfies the constraint on $\bar{\Lambda}$ set in Ref. [2,3] when $\lambda_{BL} = 0$. Indeed, $\bar{\Lambda} > 1000$ if these were GM1 stars with $\lambda_{BL} = 0$. However, when $\lambda_{BL} \neq 0$ the value of $\bar{\Lambda}$ falls by a large amount for both EOSs, so much so that it can lie within the GW-EM bounds for a certain amount of pressure anisotropy. Furthermore, the lower bound on $\bar{\Lambda}$ helps limit the value of λ_{BL} from above. In the right panel of Fig. 5 the allowed ranges of λ_{BL} are plotted against q for DDHδ (upper panel) and GM1 (lower panel) EOSs. We find that presence of anisotropy in pressure can reduce the value of Λ by a significant amount. Thus, certain EOSs that were ruled out by GW170817 observations for $\lambda_{BL} = 0$ become viable if the stars support an anisotropic component in the pressure.

It is important to note that, GW170817 was undoubtedly hot near merger and post merger. Therefore, the limit $\bar{\Lambda} > 400$ may be potentially affected by details such as whether hot equations of state are considered in the late inspiral and merger phases of the binary.

A. Using universality relations for further constraining pressure anisotropy

As shown in Fig. 4 in the mass range of interest $[1, 2]\ M_{\odot}$, in the presence of positive pressure anisotropy the tidal Love number decreases for any fixed stellar mass. Thus, the Λ distribution of stars with a soft EOS, such as SLy4 with no pressure anisotropy, can be difficult to distinguish from that of stars with a stiff EOS, such as DDHδ, but nonzero pressure anisotropy, say, $\lambda_{BL} = .59$; see the left panel of Fig. 6. In this sense, positive anisotropy has an effect that is similar to making a star softer, for a given mass. This poses the problem of how one might distinguish these two types of stars. We argue

here that it is possible to make the correct identification in some cases by measuring the stellar radius. This is because a nonzero λ_{BL} tends to make the star larger, for any fixed stellar mass (see the right panel of Fig. 6). Note there that DDHδ with $\lambda_{BL} = .59$ has a larger radius for most of the mass range than SLy4 with any $\lambda_{BL} \in [0, 2]$.

To measure the stellar radius, we adopt the same trick that was resorted to in Ref. [2], namely, to use universality relations between Λ and stellar compactness. Universality of the $C - \Lambda$ relationship was first pointed out by Maselli et al. [49]. Here, we inspect whether this universality also holds in the presence of pressure anisotropy, Eq. (5). In the top left panel of Fig. 7, C vs $\ln \Lambda$ is plotted for five different isotropic EOSs. We find that C is well fitted by the following relation,

$$C = 0.356883 - 0.0363734 \ln \Lambda + 0.000899844 (\ln \Lambda)^2.$$
(12)

GW170817 has constrained the value of Λ for a 1.4 $M_{\odot}$ star to be 190^{+390}_{-120} [2]. If we use the above mentioned $C - \Lambda$ relationship and this constraint on Λ, then the radius of the two stars in GW170817 is measured to be $10.8^{+2.0}_{-1.4}$ km, with the upper limit consistent with Ref. [2], and the lower limit larger by 0.3 km at most.

In the top right panel of Fig. 7, C vs $\ln \Lambda$ is plotted for different EOSs but with fixed $\lambda_{BL} = 0.59$. We observe universality relation holds, in fact somewhat more tightly, for such pressure anisotropy. The fitted $C - \Lambda$ relation for this anisotropic configuration is

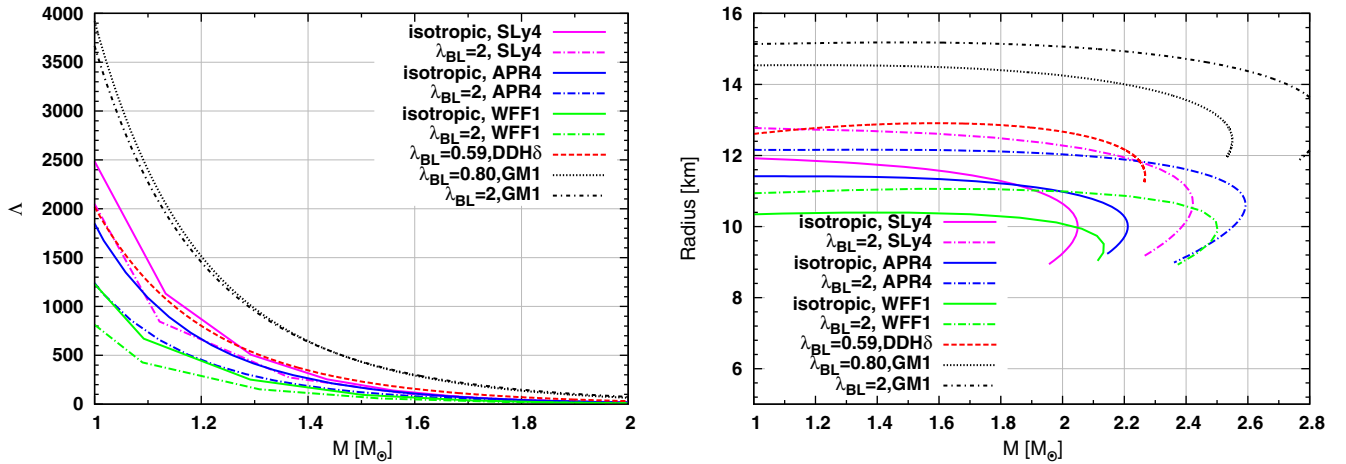$$C = 0.349945 - 0.0382978 \ln \Lambda + 0.00106643 (\ln \Lambda)^2,$$
(13)

FIG. 6. Dimensionless tidal deformability Λ (left panel) and radius (right panel) is plotted as a function of mass: The solid lines correspond to isotropic neutron stars (black, blue and green are respectively for Sly4, Apr4 and Wff1 EOSs) and the red dotted line corresponds to DDHδ stars but with EOS anisotropic pressure $\lambda_{BL} = .26$.
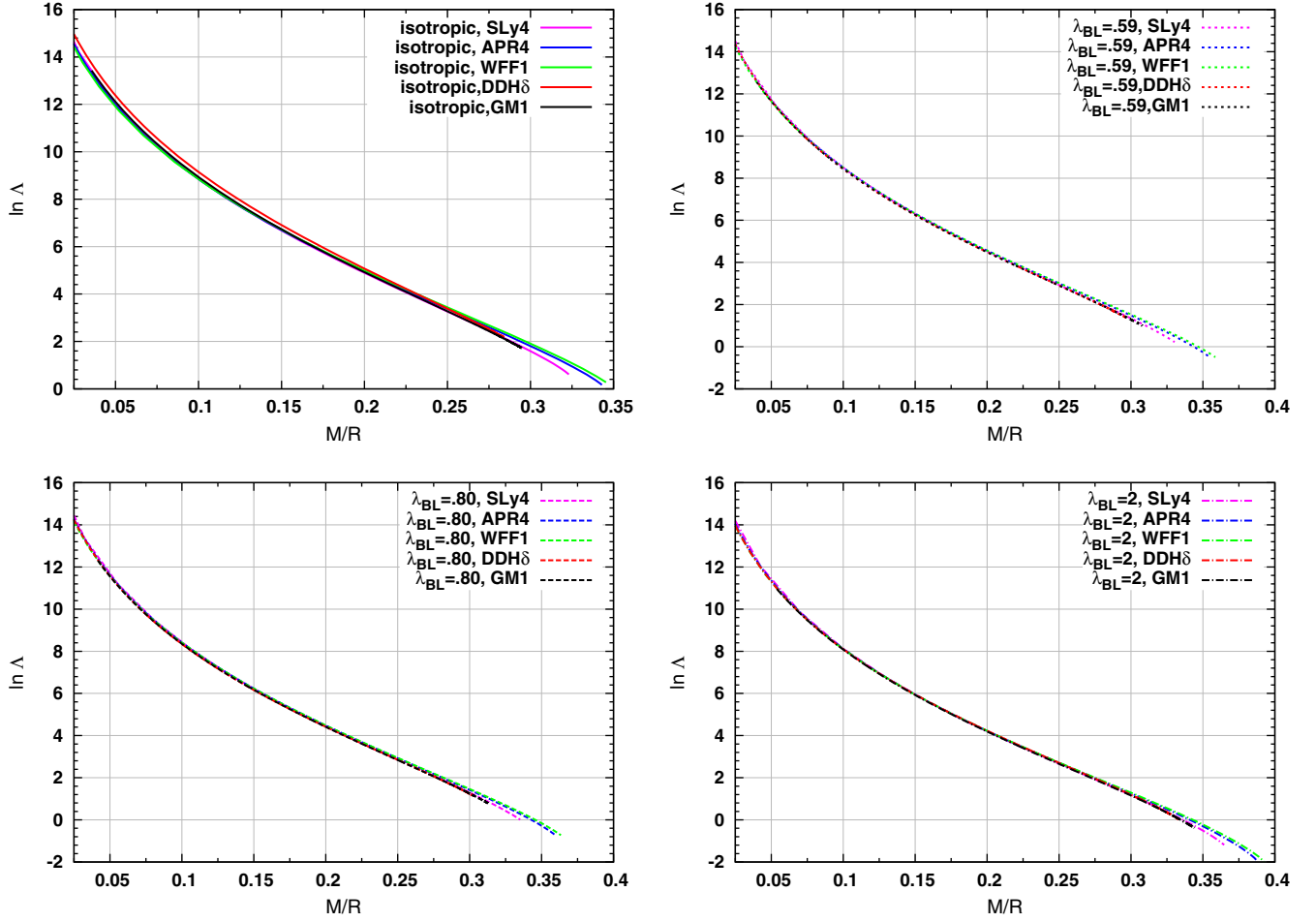
FIG. 7. $C - \Lambda$ relationship for different cases: different EOSs with $\lambda_{BL} = 0$ (top left), different λ_{BL} for fixed DDHδ EOS (top right), different EOSs with $\lambda_{BL} = 1$ (bottom left), different EOSs with $\lambda_{BL} = 2$ (bottom right).

and the radius is constrained to $11.6^{+2.2}_{-1.6}$ km for the same Λ measurement of 190^{+390}_{-120}. With $\lambda_{BL} = 0.80$ (bottom left panel),

$$C = 0.347709 - 0.0384087 \ln \Lambda + 0.00108876 (\ln \Lambda)^2,$$
(14)

and the radius will be constrained to $11.7^{+2.3}_{-1.6}$ km for the aforementioned Λ. With $\lambda_{BL} = 2$ (bottom right panel),

$$C = 0.337864 - 0.0367376 \ln \Lambda + 0.000985149 (\ln \Lambda)^2,$$
(15)

and the radius is found to be $12.0^{+2.3}_{-1.6}$ km.

We illustrate in Table I how the above radius measurements can be used to rule in or out various EOSs with nonzero λ_{BL}. For example, the universality relation Eq. (13) implies that for DDHδ neutron stars with the same masses as GW170817, and $\lambda_{BL} = .59$, the radius must obey $11.6^{+2.2}_{-1.6}$ km (90% CL), which allows for the maximum radius of such stars to be 13.8 km. However, Fig. 6 shows

that the minimum radius for such a star in the 1–2 $M_\odot$ mass range is $R_{min} = 12.7$ km, which is less than 13.8 km. This is why we infer that DDHδ remains viable following the observation of GW170817 provided $\lambda_{BL} \geq 0.59$.

TABLE I. Use of radius constraints to discern the presence or absence of pressure anisotropy. For example, the universality relation Eq. (13) implies that for DDHδ neutron stars with the same masses as GW170817, and $\lambda_{BL} = .59$, the radius must obey $11.6^{+2.2}_{-1.6}$ km (90% CL), which allows for the maximum radius of such stars to be 13.8 km. However, Fig. 6 shows that the minimum radius for such a star in the 1–2 $M_\odot$ mass range is $R_{min} = 12.7$ km, which is less than 13.8 km. This is why we infer that DDHδ remains viable following the observation of GW170817 provided $\lambda_{BL} \geq 0.59$.

EOS	Degree of anisotropy	Bound on radius	R_{min} (km)	Comment
DDHδ	$\lambda_{BL} = .59$	$11.6^{+2.2}_{-1.6}$	12.7	Survive
GM1	$\lambda_{BL} = .80$	$11.7^{+2.3}_{-1.6}$	14.2	Ruled out
GM1	$\lambda_{BL} = 2$	$12.0^{+2.3}_{-1.6}$	15.1	Ruled out

Note that DDHδ with $\lambda_{BL} \geq 0.59$ is allowed by the GW-EM constraint on $\bar{\Lambda}$, as already observed in Fig. 5. On the other hand, the universality relation Eq. (14) implies that for GM1 neutron stars with the same masses as GW170817, and $\lambda_{BL} = .80$, the radius must obey $11.7^{+2.3}_{-1.6}$ km (90% CL), which allows for the maximum radius of such stars to be 14.0 km. However, Fig. 6 shows that the minimum radius for such a star in the 1–2 $M_\odot$ mass range is $R_{\min} = 14.2$ km, which is larger than 14.0 km. This is why we infer that GM1, with $\lambda_{BL} \geq 0.80$, is ruled out following the observation of GW170817.

In the analysis of the GW170817 signal in Ref. [2], LIGO and Virgo used another factor, arising from pulsar mass observations, namely that any viable EOS must support NS with a maximum mass that is at least 1.97 $M_\odot$. This requirement gives an improved measurement of radius. We leave the study of the corresponding impact in λ_{BL} constraints to a future study.

We also observe that more observations of neutron star mergers, as anticipated, will help constrain λ_{BL} more tightly. This will help in narrowing the statistical errors, thereby allowing smaller systematic effects arising from λ_{BL} to stand out. Indeed, when the statistical error of any GW observable gets so precise (e.g., with larger number of observations) that it is smaller than the systematic shift induced by nonzero λ_{BL}, then it becomes meaningful to use it to constrain the presence of anisotropic pressure in these stars.

Note that there are preliminary indications from numerical relativity simulations that the ejecta mass from such mergers is correlated with the neutron star equation of state or radius [50] and might be estimated precisely enough from the luminosity of any electromagnetic emission it fuels. As these simulations mature and their results become more reliable, they have the potential to provide an additional channel for measuring these parameters and, perhaps, aid in constraining anisotropy.

V. CONCLUSION

In this paper, we have calculated tidal Love number and deformability of neutron stars in the presence of anisotropic pressure. As a first step, we use two RMF EOSs to describe radial pressure and a functional form of anisotropic pressure as proposed by Bowers and Liang [19]. We obtain the equilibrium solutions numerically by integrating modified TOV Eqs. (3) and (4), and find that they can differ significantly from the isotropic ones: We observe that for any fixed central density, the compactness of the star increases for positive anisotropy ($\lambda_{BL} > 0$) and decreases for negative anisotropy ($\lambda_{BL} < 0$). In a further investigation, when we plot transverse pressure as a function of radius for the chosen negative values of λ_{BL} we notice that the $p_t \geq 0$ requirement is not met everywhere inside the

star. Therefore, we discard those anisotropic EOSs with negative values of λ_{BL}.

The tidal Love numbers and deformabilities are obtained by integrating the single Eq. (9) for the perturbed metric variable H, along with the modified TOV Eqs. (3) and (4), and for the boundary condition $p(r = R) = 0$. It turns out that both tidal Love numbers and deformabilities can reduce by a significant amount in the presence of pressure anisotropy. This leads to an interesting possibility. Earlier, a subset of those EOSs that failed to satisfy the bound of tidal deformability set by GW170817, can now become viable if anisotropy in pressure is present beyond a certain threshold. We demonstrate this by analyzing the cases of two RMF EOSs, DDHδ and GM1, for various values of λ_{BL}. Finally we propose how future observations may be able to discern the presence or absence of anisotropic pressure. However, there is scope to extend this study for a spinning object. Tidal deformation of a spinning object has been studied in case of isotropic star [51,52]. These studies show that value of tidal deformability increases by 10%. So, spin has the opposite effect compared to anisotropy. This is why we have studied isotropy alone here. Adding spin can be pursued in the future.

ACKNOWLEDGMENTS

APPENDIX: COMMENT ON ANISOTROPIC ULTRACOMPACT OBJECTS

Positive anisotropy parameter yields higher compactness. It has been argued that by increasing the value of the anisotropic parameter sufficiently the black hole limit can be reached [38,39]. But one should carefully examine how the transverse pressure behaves for those high anisotropic parameters. In the left panel of Fig. 8 transverse pressure is plotted as a function of radius using DDHδ and $\lambda_{BL} = 4$ for different values of central energy density. We observe transverse pressure increases with the radius and finally near the surface it starts decreasing and vanishes at the surface. In order to obtain such behavior for the transverse pressure we need some exotic physical phenomenon that enhances the value of the transverse pressure. But in reality, we do not expect such type of physical processes. In the right panel of Fig. 8
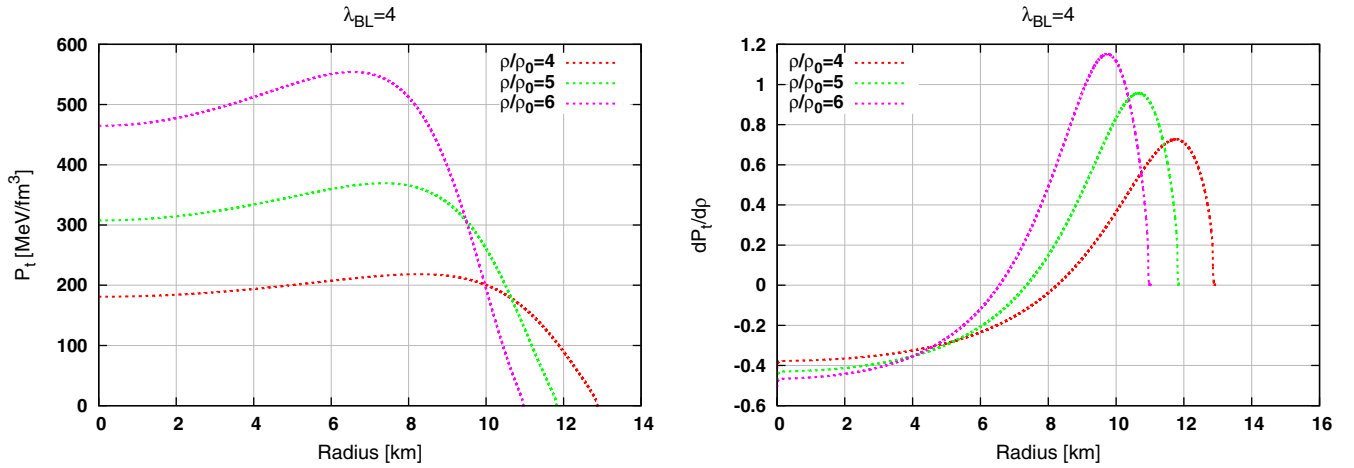
FIG. 8.   Radial profile of transverse pressure is plotted for different values of central density using DDHδ EOS and $\lambda_{BL} = 4$ (left panel). Corresponding transverse sound speed is plotted as a function of radius (right panel).

radial profile of the transverse sound speed squared (defined as, $c_{s,t}^2 = \frac{dp_t}{d\rho}$) is plotted for the same configuration used in left panel. The region where the transverse pressure increases with r, the transverse sound speed becomes negative. Also, for higher central density (here, $\frac{\rho}{\rho_0} = 6$) transverse EOS becomes acausal. So, clearly, it is physically not possible to achieve the black hole limit by increasing the degree of anisotropy.

[1] B. P. Abbott *et al.* (LIGO Scientific and Virgo Collaborations), Phys. Rev. Lett. **119,** 161101 (2017).

[2] B. P. Abbott *et al.* (LIGO Scientific and Virgo Collaborations), Phys. Rev. Lett. **121,** 161101 (2018).

[3] B. P. Abbott *et al.* (LIGO Scientific and Virgo Collaborations), Phys. Rev. X **9,** 011001 (2019).

[4] D. Radice, A. Perego, and F. Zappa, Astrophys. J. **852,** L29 (2018).

[5] É. É. Flanagan and T. Hinderer, Phys. Rev. D **77,** 021502 (2008).

[6] T. Hinderer, Astrophys. J. **677,** 1216 (2008).

[7] T. Binnington and E. Poisson, Phys. Rev. D **80,** 084018 (2009).

[8] T. Damour and A. Nagar, Phys. Rev. D **80,** 084035 (2009).

[9] L. Herrera and N. O. Santos, Astrophys. J. **438,** 308 (1995).

[10] R. Kippenhahn, A. Weigert, and A. Weiss, *Stellar Structure and Evolution* (Springer, New York, 2012).

[11] M. Ruderman, Annu. Rev. Astron. Astrophys. **10,** 427 (1972).

[12] V. Canuto and S. M. Chitre, Phys. Rev. D **9,** 1587 (1974).

[13] R. F. Sawer, Phys. Rev. Lett. **29,** 382 (1972).

[14] J. B. Hartle, R. F. Sawyer, and D. J. Scalapino, Astrophys. J. **199,** 471 (1975).

[15] K. Hurley *et al.,* Nature (London) **397,** 41 (1999).

[16] C. Kouveliotou *et al.,* Nature (London) **393,** 235 (1998).

[17] L. D. Landau and E. M. Lifshitz, *Fluid Mechanics* (Pergamon Press, London, 1959), p. 507.

[18] K. Chakravarti, S. Chakraborty, S. Bose, and S. SenGupta, Phys. Rev. D **99,** 024036 (2019).

[19] R. Bowers and E. Liang, Astrophys. J. **188,** 657 (1974).

[20] M. Cosenza, L. Herrera, M. Esculpi, and L. Witten, J. Math. Phys. (N.Y.) **22,** 118 (1981).

[21] B. W. Stewart, J. Phys. A **15,** 2419 (1982).

[22] S. Bayin, Phys. Rev. D **26,** 1262 (1982).

[23] K. D. Krori, P. Borgohain, and R. Devi, Can. J. Phys. **62,** 239 (1984).

[24] S. D. Maharaj and R. Maartens, Gen. Relativ. Gravit. **21,** 899 (1989).

[25] H. Bondi, Mon. Not. R. Astron. Soc. **259,** 365 (1992).

[26] R. Chan, L. Herrera, and N. Santos, Mon. Not. R. Astron. Soc. **265,** 533 (1993).

[27] M. K. Gokhroo and A. L. Mehra, Gen. Relativ. Gravit. **26,** 75 (1994).

[28] L. K. Patel and N. P. Mehta, Aust. J. Phys. **48,** 635 (1995).

[29] L. Herrera, A. Di Prisco, J. Ospino, and E. Fuenmayor, J. Math. Phys. (N.Y.) **42,** 2129 (2001).

[30] T. Papakostas, Int. J. Mod. Phys. D **10,** 869 (2001).

[31] M. K. Mak, P. N. Dobson, and T. Harko, Int. J. Mod. Phys. D **11,** 207 (2002).

[32] B. V. Ivanov, Phys. Rev. D **65,** 104011 (2002).

[33] T. Harko and M. K. Mak, Proc. R. Soc. A **459,** 393 (2003).

[34] H. Hernandez and L. A. Nunnez, Can. J. Phys. **82,** 29 (2004).

[35] D. D. Doneva and S. S. Yazadjiev, Phys. Rev. D **85,** 124023 (2012).

[36] H. O. Silva, C. F. B. Macedo, E. Berti, and L. C. B. Crispino, Classical Quantum Gravity **32,** 145008 (2015).

[37] K. Yagi and N. Yunes, Phys. Rev. D **91,** 123008 (2015).

[38] K. Yagi and N. Yunes, Phys. Rev. D **91,** 103003 (2015).

[39] K. Yagi and N. Yunes, Classical Quantum Gravity **33,** 095005 (2016).

[40] J. D. V. Arbañil and M. Malheiro J. Cosmol. Astropart. Phys. 11 (2016) 012.

[41] G. Raposo, P. Pani, M. Bezares, C. Palenzuela, and V. Cardoso, arXiv:1811.07917.

[42] T. Gaitanos, M. Di Toro, S. Typel, V. Baran, C. Fuchs, V. Greco, and H. H. Wolter, Nucl. Phys. **A732,** 24 (2004).

[43] N. K. Glendenning and S. A. Moszkowski, Phys. Rev. Lett. **67,** 2414 (1991).

[44] F. Douchin and P. Haensel, Astron. Astrophys. **380,** 151 (2001).

[45] K. S. Thorne and A. Campolattaro, Astrophys. J. **149,** 591 (1967).

[46] T. Regge and J. A. Wheeler, Phys. Rev. **108,** 1063 (1957).

[47] E. Annala, T. Gorda, A. Kurkela, and A. Vuorinen, Phys. Rev. Lett. **120,** 172703 (2018).

[48] R. Nandi, P. Char, and S. Pal, arXiv:1809.07108.

[49] A. Maselli, V. Cardoso, V. Ferrari, L. Gualtieri, and P. Pani, Phys. Rev. D **88,** 023007 (2013).

[50] S. Ascenzi, N. D. Lillo, C. J. Haster, F. Ohme, and F. Pannarale, arXiv:1808.06848.

[51] P. Pani, L. Gualtieri, and V. Ferrari, Phys. Rev. D **92,** 124003 (2015).

[52] P. Landry, Phys. Rev. D **95,** 124058 (2017).